International Journal of Sciences: Basic and Applied Research (IJSBAR)

ISSN 2307-4531
(Print & Online)

http://gssrr.org/index.php?journal=JournalOfBasicAndApplied

The Distribution of 870 µm Continuum, CO(3-2) and HCO^+(4-3) Molecules Around TW HYA, Based on Science Verification Data from ATACAMA Large Millimeter/Submillimeter Array (ALMA), Band 7 Data

Abdulrahman Malawi[a]*, Dalal Al Ghamdi[b]

[a,b]*Astronomy department, King Abdulaziz University, Jeddah*

[a]*Email: amalawi@kau.edu.sa*

[b]*Email: dalal_jalal@hotmail.com*

Abstract

The study of the chemistry of protoplanetary disks has broad implication for our understanding of planet compositions and the availability of the conditions necessary for life. The science verification data from the Atacama Large Millimeter/submillimeter Array (ALMA) band 7 (345 GHz) observation of TW Hya, a classical T Tauri star, at lines of HCO^+ (4-3) and CO (3-2) with a 1.5" angular and 0.2km/s spectral resolution was used for this study. CASA, the common astronomy software applications package was used for the data reduction, including, calibrating, cleaning and imaging of both spectral line and the continuum. The final dust, CO(3-2) and HCO^+(4-3) images of the disk and the corresponding models are presented and discussed.

Keywords: Circumstellar; individual(TWHydra); protoplanetary disks; submillimeter; stars; molecular processes.

1. Introduction

TW Hydrae Association (TWA) provides an excellent ground in which to study the evolution of protoplanetary dusty disks. It consists of more than 24 star systems within 40pc of each other [1, 2, 3, 4, 5].

---

* Corresponding author.

It is also, known to be one of the closest (60pc) young stellar groups to Earth. Primary members range in spectral type from A0 to M3 and have common ages of 5-10 Myr, as determined from the pre-main sequence tracks, Li abundances and X-ray fluxes. Thus, TWA stars are poised between T Tauri and main sequence stages of the stellar evolution.

TW Hya is the best starting point for understanding protoplanetary disks and their chemistry. At a distance of 54.6 pc [6], it is, in fact, the closest protoplanetary disk to Earth, surprisingly, residing far from any known molecular cloud. The spectral type of TW Hya is K6 [2, 7]. All these facts put TW Hya upfront all other protoplanetary disk candidates. Given its roughly solar-mass central star, the circumstellar environment is likely similar to that of the early solar system, with the important and intriguing caveat that TW Hya is a single star with a mass of 0.8 $M_{\odot}$ [8]. The disks retain substantial reservoirs of molecular gas , estimates, as much as 0.050 $M_{\odot}$. of CO and other trace molecular species detected and mapped thus far [e.g., 9, 10, 11, 12, 13, 14, 8, 15]. It's nearly face-on geometry eliminates many degeneracies and complications associated with studying molecular distributions around highly inclined disks. The morphology of TW Hya's dust has been the subject of several studies, including those made by [16, 17, 18, 19, 14]. The density and temperature profiles of the star and the disk are also well-constrained. Among those purposes which make observing and studying TW Hay so important are: the evolved population of the disk's solids, with a radially concentrated population of larger grains (cm) size particles near the midplane of the disk [20, 16], and a sharp radial decrease in the solids-to-gas mass ratio [8], who announces substantial growth and inward migration. The depletion of the microwave emission due to the radial drift [21] does not agree with the advanced age of TW Hya (~10 Myr), it is also, not in consistent with the assumption of a globally negative pressure gradient. There is an evidence for substructure in this disk, including a central depletion [22, 23] and the tentative signatures of "gaps" or "breaks" in the infrared scattered light emission [24,19,17,18,14]. The optical/near-infrared scattered light observations with VLT/SPHERE confirms the ∼24 au gap, as well as a clearing at ∼1. 005, or 88 au. All these findings are open questions that needs to be addressed. Therefore, establishing the importance of studying the molecular chemistry and disk dissipation processes of the dust and gas orbiting TW Hya is very important.

Studying the outer cold disk at Millimeter and submillimeter have been proved to be very useful in revealing the kinematic and physical properties of the disk. For example, previous observations by VLA at 7 mm [26], ATCA at 3 mm [20], and SMA at 1.3, 0.87, and 0.45 mm [10,11,12,27] reveal Keplerian rotation in the disk and an inclination angle of about 7 degrees. The Atacama Large Millimeter Array (ALMA) is used to study the 870 μm dust continuum, with the long baselines to trace millimeter-sized particles in the disk, down to spatial scales of 1 AU as well as the CO(3-2) and HCO^{+}(4-3) molecular lines. In an attempt to look for planets around TWHya, [28] made a deep imaging search for planets forming in the protoplanetary disk, using the KECK/NIRC2 VORTEX CORONAGRAPH.

Here, we present the data from ALMA observations of the TWHya disk covering the CO J=3–2 and HCO^{+} J=4-3 lines and the dust continuum. The maximum resolution is 1.5 ". Resulting images unambiguously reveal the rotation of the disk around the star and constrain the disk inclination and size. Section 2 presents the ALMA observations and data reduction. The results of these observations are outlined in Section 3. Section 4 presents the discussion of the results. Conclusions are given in Section 5..

2. Observations and data reduction

The observations of TWHya at Band 7 (frequency of about 345 GHz) were carried out on April 22, 2011. 9 antennas were available, although one has to be flagged. The baseline lengths ranged between 16.6 and 91.02 m.

Three sets of 1.5 hours long were run in a row, for a total of about 4.5 hours of observing time. ALMA's correlator was configured to record dual polarization with four separate spectral windows (basebands). Two basebands were placed in the lower sideband (LSB) and the other two basebands in the upper sideband (USB). In the LSB the CO(3-2) line at a rest frequency of 345.79599 GHz is located, in spw=2. In the USB the HCO^+(4-3) line at a rest frequency of 356.7342 GHz is located, in spw=0. The other two spectral windows do not contain strong spectral lines and they are used for measuring the continuum. Each spectral window is 0.5 GHz wide and the channel width is 122 kHz. Because ALMA's correlator was configured to apply Hanning smoothing of the signal, the effective spectral resolution is about twice the channel width, which in this case is about 0.2 km/s. For the antenna configuration in use at the time, the angular resolution is expected to be about 1.5". The median value of precipitable water vapor (PWV) for this period was 1.16 mm, as measured by the water vapor radiometers. This PWV corresponds to an opacity of 0.20 at the CO(3-2) line. The mean wind speed was 6.2 m/s.

We calibrated the ALMA data, using CASA (Common Astronomy Software Applications) software package. The flux scale was determined by observations of Titan, while the source 3c279 was used as a frequency-dependent bandpass calibrator. Quasars J1037-295 and J1147-382 were used as primary and secondary phase calibrators, respectively. All the above observations were carried out alternatively, with the observations of TWHya. Each of the three-data set was reduced separately and then combined together prior to imaging. The composite visibilities were Fourier inverted, deconvolved with CLEAN algorithm, and image was restored with a synthesized beam using CASA software package. The intensity maps were then, produced. Finally, we used the ALMA simulator from the CASA package, to make predictions of what ALMA will see for a given wavelength, angular resolution, and integration time, for disks at a specific distance, declination and inclination, we use the.

3. Results

3.1. Continuum image

The synthesized continuum map for TWHya is shown in Figure 1. The map covers 9 arc seconds on each side, corresponding to 491 AU at the adopted distance of 54.6 pc [6]. Simple model, IMFIT task, is performed to fit single gaussian component to the continuum. The result shows the following:

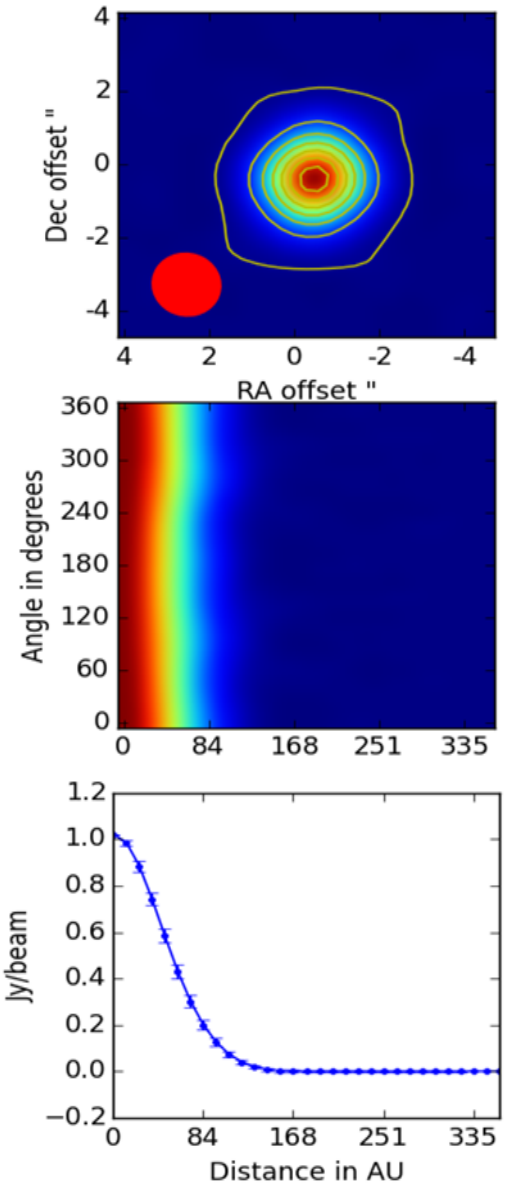

Figure 1: Top panel shows the continuum line distribution of the disk of TW Hay, the middle panel is deprojected map in polar coordinate of the disk and bottom panel is the azimuthally averaged radial surface brightness profile. Contour levels start at 0.01with 1 (Jy/beam) spacing

The image component convolved with the synthesized beam (1.68 X 1.56 arcsec at position angle 23.7 deg.) is found to have a FWHM of 1.9928 X 1.8919 arcsec, corresponding to 108.8 X 103.29 AU. This indicates that the emission is spatially unresolved, implying that the bulk of the emission comes from a region smaller in diameter. The deconvolved image size at FWHM is 1.066 X 1.063 arcs, corresponding to 58.2 X 58.039 AU. The almost, circular shaped, deconvolved image size is in agreement with the continuum size found by [14] who

studieded the same object with a much higher angular resolution (synthesized beam), it also, agrees with the previous SMA observations [29] and other ALMA observations. The total flux is 1.4346 Jy, and the peak flux is 1.0028 Jy/beam. The measured rms 0f 1.3 mJy/beam is found to be four times the theoretical value of 0.3 mJy/beam. This is likely due to residual sources of non-closing errors in the data like, baseline errors and baseline-dependent bandpass errors. Polarization errors, which we did not calibrate at all, can also, contribute, as well as imperfect uv-coverage with only 8 antennas. The mid panel shows the synthesized map deprojected to polar coordinate system. The radial profile of the surface brightness is shown in lower panel.

The estimated dust mass is calculated, using:

$$M_{dust} = \frac{F_v x D^2}{K_v B_v(T_{dust})} \qquad (1)$$

Reference [30], where D is the distance, $K_v = 1.15\ {}^{cm^2}/_{gm}$ [13] is adapted, and the estimated dust mass is fourd to be

$M_{dust} = 62.434\ M_{\oplus}$, or $M_{dust} = 1.874\ x\ 10^{-4}\ M_{\odot}$

3.1.1. Dust modeling

The photometric data of TWHya, spanning the optical to mm-length spectral region are presented in Table 1.

The data was obtained from VizieR site, which provides access to the most complete library of published astronomical catalogs and data tables available on line, organized in a self-documented database. Our data is also, included in the table.

These data are used to construct the spectral energy distribution (SED), with the best fitted model shown in Figure 2.

The SED shows a clear IR excess and the IR luminosity is larger than the optical luminosity. This is a typical characteristic of protostars belonging to the class II SED [31]. It is interpreted in terms of a spherical envelope and regarded as a classical T Tauri Stars (CTTS) with a protoplanetary disk.

We studied the physical density and temperature structure of the disk surrounding TWHya, by fitting the SED,

using, Hyperion, a three-dimensional dust continuum Monte-Carlo radiative transfer code [32] to properly estimate the physical parameters of the dust disk surrounding the central star.

Table 1: The photometric data of TWHya

Wave length (micron)	$\lambda f\lambda(\frac{\text{ergs}}{\text{sec.}\,cm^2})$	Filter
4.20E-01	4.10E-10	HIP:BT
4.44E-01	5.01E-10	Johnson:B
4.82E-01	4.91E-10	SDSS:g'
5.32E-01	6.14E-10	HIP:VT
5.54E-01	8.19E-10	Johnson:V
6.25E-01	1.21E-09	SDSS:r'
7.63E-01	1.38E-09	SDSS:i'
7.90E-01	1.68E-09	DENIS:I
1.24E+00	1.96E-09	2MASS:J
1.25E+00	1.99E-09	Johnson:J
1.63E+00	1.81E-09	Johnson:H
1.65E+00	1.77E-09	2MASS:H
2.16E+00	1.1E-09	2MASS:Ks
2.19E+00	1.08E-09	Johnson:K
3.35E+00	4.02E-10	WISE:W1
4.49E+00	1.78E-10	Spitzer/IRAC:4.5
4.60E+00	1.87E-10	WISE:W2
8.61E+00	1.57E-10	AKARI:S9W
1.16E+01	1.51E-10	WISE:W3
1.20E+01	1.66E-10	:=12um
1.84E+01	2.36E-10	AKARI:L18W
2.21E+01	2.79E-10	WISE:W4
2.39E+01	3.07E-10	IRAS:25
2.50E+01	2.96E-10	:=25um
6.00E+01	1.96E-10	:=60um
6.18E+01	1.91E-10	IRAS:60
1.00E+02	1.54E-10	:=100um
1.02E+02	1.46E-10	IRAS:100
1.40E+02	1.36E-10	AKARI:WIDE-L
3.50E+02	5.97E-11	@{Freq}
5.50E+02	2.08E-11	:=545GHz
8.49E+02	5.54E-12	:=353GHz
8.54E+02	5.07E-12	This work
8.55E+02	4.2E-12	SCUBA:850
1.30E+03	2.02E-12	:=1.3mm
1.38E+03	1.25E-12	:=217GHz

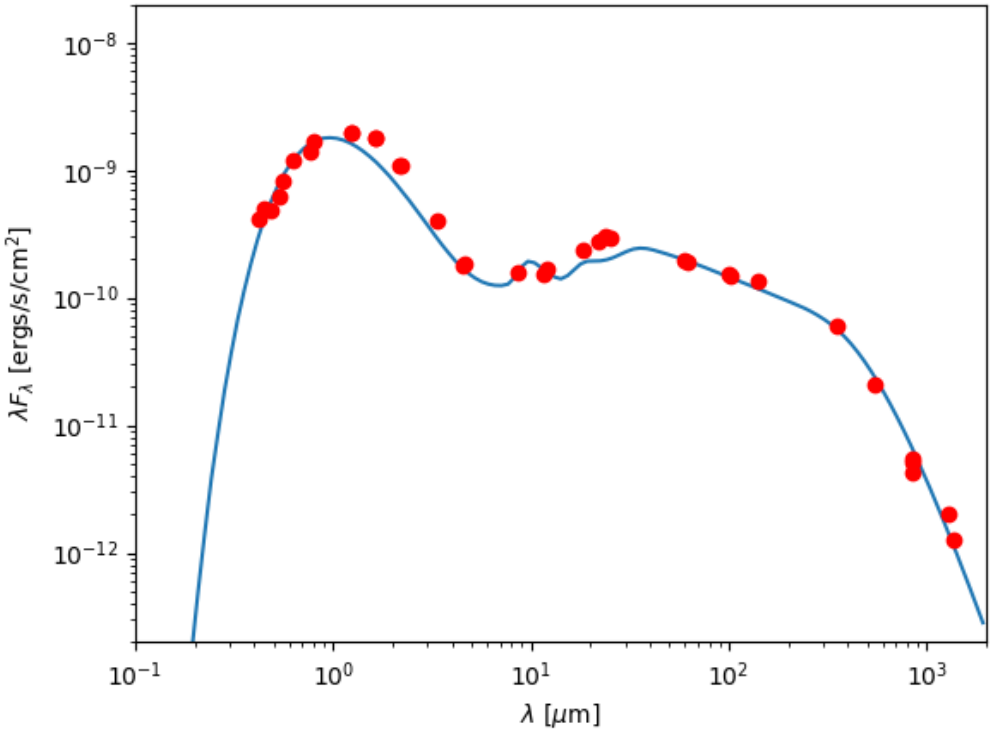

Figure 2: Comparison of the model structures in Table 2 with observations of the dust continuum emission from the TW Hya disk.

The central source is a point source with a 3800 K blackbody spectrum, and a radius of 1.1 $r_\odot$. The disk extends from 0.4 to 150 AU, and has a flared disk density structure given by:

$$\rho(r,z) = \rho_o \left(\frac{r}{r_o}\right)^{-b} \exp\left[\frac{-1}{2}\left(\frac{z}{h_o\left({}^{r}/_{r_o}\right)^{\beta}}\right)^2\right] \qquad (2)$$

where

r is the cylindrical polar radius, $h_\circ$ is the vertical height. from midplane. $r_\circ = r_\odot$, $h_\circ = 0.0175\, r_\odot$, b = -1., and β = 1.125. The disk is made up of dust grains with a power law size distribution, and composed of astronomical silicates and graphite, grain particles, with the properties of the grains given by [33].

The best fitting parameters are shown in table 2.

Table 2: The best fitting parameters

Central Source Parameters	
$R_\star$	1.1 $R_\odot$
$T_\star$	3800 K
Disk Parameters	
M_{disk}	0.005 $M_\odot$
r_{min}	0.4 AU
r_{max}	150 AU
$r_\circ$	$R_\star$
$h_\circ$	0.0175 $r_\circ$
b	-1
β	1.15

3.2. CO (J= 3-2) line

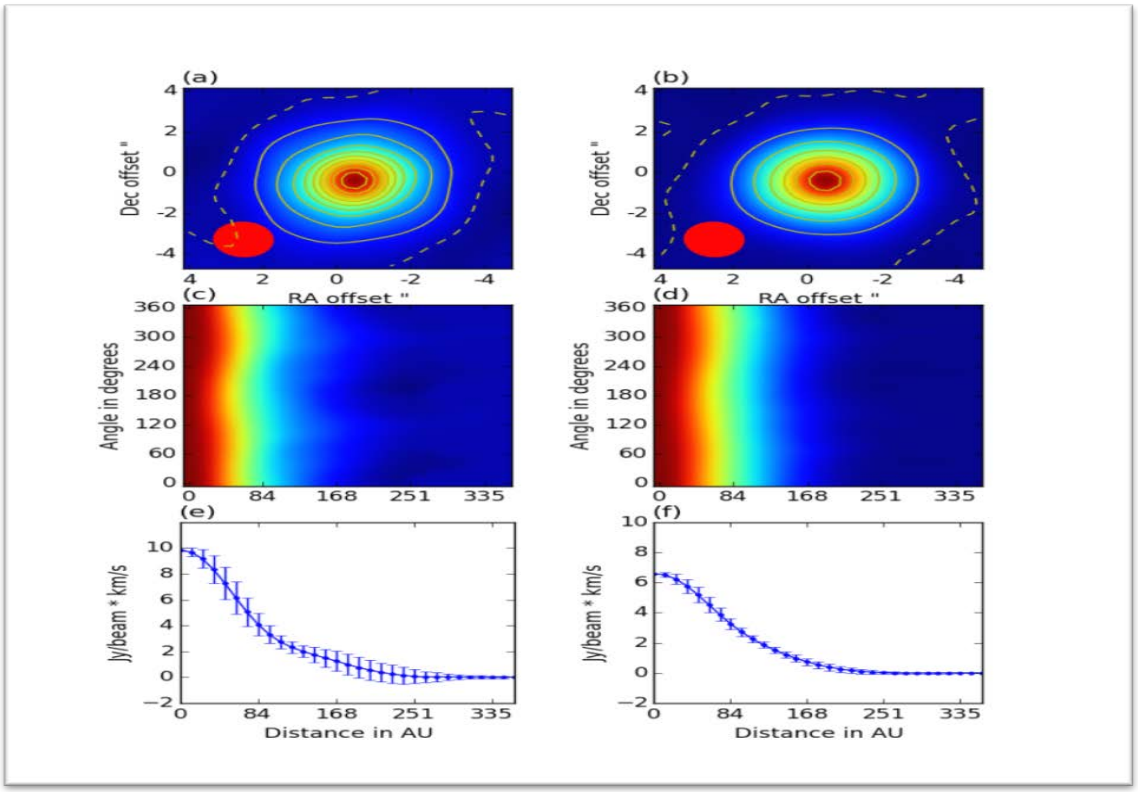

Figure 3: panel (a) and (b) show the integrated flux density of CO(3-2) and HCO^+(4-3) lines, respectively. The deprojected maps for CO(3-2) and HCO^+(4-3) are shown in panel (c) and (d), respectively. Panel (e) and (f) are the radial view of the two deprojected maps. Contour levels start at 0.001with 1 (Jy/beam * km/s) spacing.

Figure 3(a) shows the integrated intensity maps of CO(3-2) line. The derpoected intensity is shown in figure3(c), and the radial profile in figure 3(e).

The integrated intensity map is fitted with simple model, using IMFIT task. Two gaussian components were used to fit the data. The result shows the following:

The size of the main component of the image, convolved with the synthesized beam (1.68 X 1.53 arcsec at position angle 22.34 deg) is found to have a FWHM of 3.936 X 3.404 arcsec, corresponding to 214.9 X 185.85 AU. This indicates that the emission is spatially unresolved, implying that the bulk of the emission comes from a region smaller in diameter. The deconvolved image size at FWHM is 3.559 X 3.039 arcsec, corresponding to 196.505 X 165.929 AU. The total integrated flux and a peak flux density for the main component are, 29.39 Jy x km/s, and 5.649 Jy/beam, respectively. The size of the second component, convolved with the same beam, at FWHM is 1.593 X 1.510 arcsec, corresponding to 86.978 X 82.446 AU. The total integrated flux and the peak flux density for the second component, are 4.12 Jy x km/s, and 4.409 Jy/beam x km/s, respectively. Both components share the same central position. The measured rms is 48.94 mJy/beam. The radial profile shows two weak gaps, the first gap is located at about 126 AU, the second is at 235 AU.

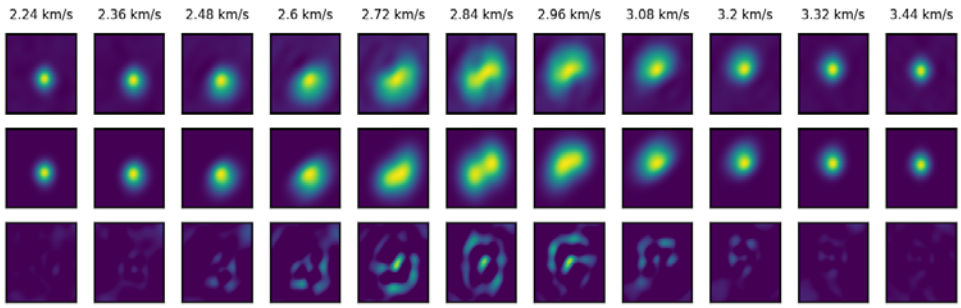

Figure 4: Upper panels shows the observed CO $J = 3 - 2$ channel maps, the fitted channel maps model is show in the middle panels, the lower panels show the residual maps.

Figure 4 shows the CO $J = 3 - 2$ channel maps from the TW Hya disk, with synthetic data from the similarity on the same angular scale as the map in panel (a) in figure 3. The channel maps show a clear rotation pattern, from northwest (blueshifted) to southeast (redshifted), with a narrow line width due to a face-on viewing geometry. Near the systemic velocity, the CO emission subtends ∼4” (215 AU) in radius

3.3. HCO^+ (J= 4-3) line

Figure 3(b) shows the integrated intensity maps of HCO^+(4-3) line, the deprojected intensity is shown in figure3(d), and the radial profile in figure 3(f).

The integrated intensity map is fitted with simple model, using IMFIT task. Two gaussian components were used to fit the data. The result shows the following:

The size of the main component of the image, convolved with the synthesized beam (1.71 X 1.6 arcsec at position angle 17.87 degree) is found to have a FWHM of 3.492 X 3.359 arcsec, corresponding to 190.663 X 183.401 AU. The deconvolved image size at FWHM is 3.048 X 2.952 arcsec, corresponding to 166.42 X 161.179 AU. The total integrated flux and the peak flux density for the main component, respectively, are 22.76 Jy x km/s, and 5.301 Jy/beam. The size of the second component, convolved with the same beam, at FWHM is 1.515 X 1.374 arcsec, corresponding to 82.719 X 75.02.446 AU. The total integrated flux and the peak flux density for the second component, respectively, are 1.045 Jy x km/s, and 1.371 Jy/beam . Both components share the same central position. The measured rms is 48.94 mJy/beam x km/s. The radial profile shows two weak rings, the first ring is located at about 126 AU, the second ring is at 235 AU. [34], used the Submillimeter Array (SMA) to make a high-resolution HCO^+(3-2) observation of TW Hya. The asymmetry shape of the resulted map showed different spatial distribution of gas in the disk from that of the HCO^+(4-3) data observed by ALMA. The possible cause of the asymmetry distribution is explained in that paper.

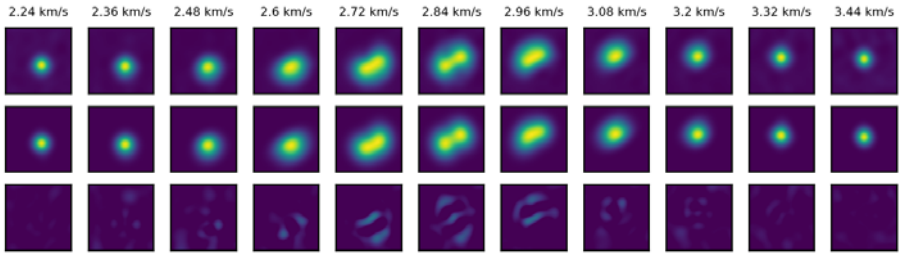

Figure 5: Upper panels shows the observed HCO^+ $J = 4 - 3$ channel maps, the fitted channel maps model is show in the middle panels, the lower panels show the residual maps

The HCO^+(4 −3) channel maps from the TW Hya disk, with synthetic data from the similarity are shown in figure 5. The angular scale is the same as the map in panel (b) of figure 3. The channel maps show a clear rotation pattern, similar to the rotation pattern seen in the CO(3-2) channel maps. Near the systemic velocity

4. Discussion

In figure 1, we show the dust continuum map in the upper panel, with the orange ellipse represents the shape and size of synthesized beam. The middle panel shows the dust continuum map deprojected to polar coordinate. The lower panel is the radial average of the deprojected map. The millimeter-sized dust structure is more compact than the CO(3-2) and HCO^+(4-3) lines [8]. Because mm-size and cm-size dust grain which are responsible for the sub-millimeter emission are concentrated in the inner part of the midplane of the disk. No gaps or rings have been detected in the continuum map, which indicates that the dust continuum is not resolved.

Figure 2 shows the SED data (red filled circles) and the fitted model (blue line). The model, seems to fit the data very well, specially the millimeter band side of the SED. We use a radiative transfer model with a sharp edge and a radially homogeneous dust composition of astronomical silicate and graphite, from small to large, grains.

Another study will follow with different approach to better represent the surface density of large grains that

concentrate towards the inner disk regions, and that of the small size grains found everywhere throughout the disk.

Figure 3, panel (a) and (b) show the integrated flux density of CO(3-2) and HCO^+(4-3) lines, respectively. The deprojected maps of the two lines are shown in panel (c) and (d), respectively. Panel (e) and (f) are the radial view of the two deprojected maps. A close inspection of the deprojected map of the CO(3-2) line reveals a gap located at about 129.5 AU, followed by another gap, located at 216 AU, and a faint data extends beyond 230 AU. The deprojected map of HCO^+(4-3), panel (d), did not show the same phenomena, although very shallow gap is seen at 129.5 AU. The gap features are similar to that found by [35] who studied the CO(3-2) line with much higher resolution using ALMA, although, the location of the gaps differs , due to the difference in the spatial resolution.

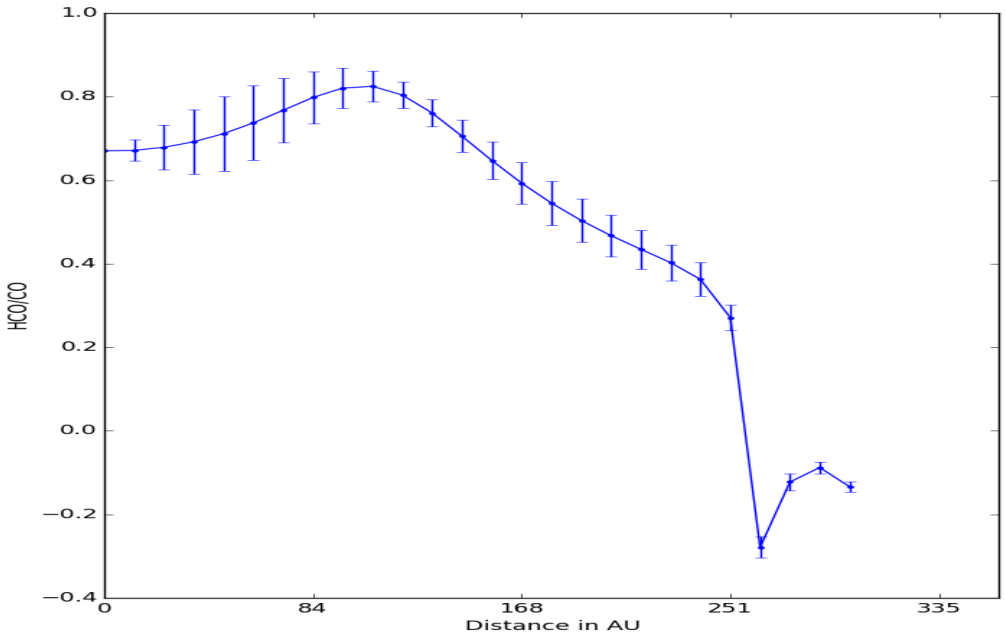

Figure 6: The HCO^+/CO ratio plotted along the radial distance

To confirm our finding, we plotted the HCO^+/CO ratio of the total integration maps, as shown in Figure 6, along the radial distance and find the following: The HCO^+/CO ratio is constant up to 12.95 AU, the ratio then begins to rise steadily and peaks at 129.5 AU, it then, decreases to 220 AU, it increases again and peaks at 230 AU. The ratio drops sharply, at 259 AU, to mark the terminate line of the HCO^+(4-3) line. Whether the two lines are optically thick, which indicates a drop in the CO(3-2) temperature, or they may also be optically thin which indicates a drop in the density of the CO(3-2) line. Both scenarios can be explained as follows:

The two peaks in the HCO^+/CO ratio profile coincide with the two gaps found in the deprojected map of CO(3-2) line, panel(c) of figure 3. This can be as a result of an increase in the HCO^+(4-3) line level, or a decrease in the CO(3-2) line emission, due to depletion in H2 line or due to CO(3-2) freeze-out on grains. The latter is most

likely to be the case as [36], stated that, the CO(3-2) depletion could indicate a general absence of H2 gas compared with dust. They pointed that, the Herschel HD observations [37] indicates that it is more likely that it is due to CO(3-2) freeze-out on grains with the possibility that subsequent grain-surface reactions form larger molecules even inside the CO(3-2) snow line [38; 39].

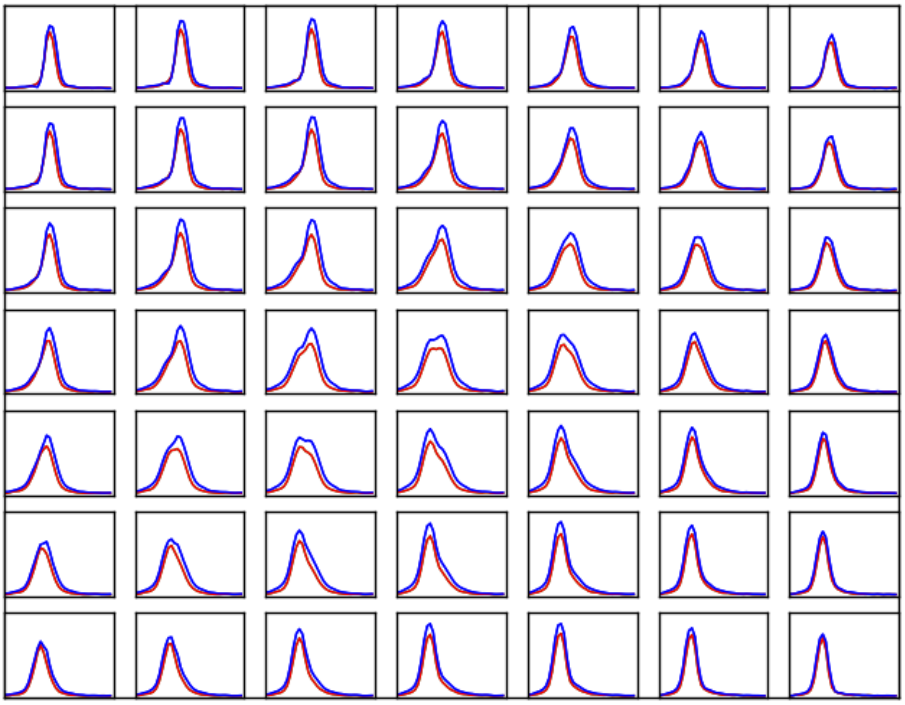

Figure 7: The CO(3-2) and HCO^+ (4-3)line profiles of the inner part of the cloud plotted on a 7 x 7 grid around the center of the map.

Finally, figure 7 shows spectral line profiles of CO(3-2), blue line, and HCO^+(4-3), red line. The plot covers 7 x 7 grid of locations around the center of the maps. The plot shows the following: the central profile shows a clear Keplerian rotation pattern, the shape of the two lines is almost the same, with some differences in the middle profiles, both in the shape as well as the strength of the lines. This could be caused by the gaps found in the CO(3-2), but not in HCO^+(4-3) disks.

There is also, a faint high velocity component, on the right side of the line. This component, that seem to be stronger in HCO^+(4-3), needs to be investigated.

5. Conclusion

From a qualitative perspective of our analyses of the radial distribution of CO(3-2) and HCO^+(4-3) lines and millimeter-sized dust grain structures in the TWHya disk, we conclude that: the millimeter-sized dust structure

is more compact than the CO(3-2) and HCO^+(4-3) lines because the millimeter size dust responsible for the dust emission is concentrated in the inner part of the disk, around the midplane of the disk. The CO(3-2) line map shows two gaps at approximately 129.5 and 220 AU. The HCO^+(4-3) line map did not show any gap or ring. The maps are not resolved. The result of fitting the SED data shows that the disk has a flared disk density structure.

Acknowledgements

This work is funded by King Abdulaziz City for Science and Technology under grant No. (1985-38-TA). This paper makes use of the following ALMA data: ADS/JAO.ALMA#2011.0.00001.SV. ALMA is a partnership of ESO (representing its member states), NSF (USA) and NINS (Japan), together with NRC (Canada), MOST and ASIAA (Taiwan), and KASI (Republic of Korea), in cooperation with the Republic of Chile. The Joint ALMA Observatory is operated by ESO, AUI/NRAO and NAOJ.

References

[1] de La Reza, R., Torres, C. A., Quast, G., Castilho, B. V. & Vieira, G. L. Discovery of new isolated T Tauri stars. The Astrophysical Journal **343**, L61-L64 (1989).

[2] Webb, R. et al. Discovery of Seven T Tauri Stars and a Brown Dwarf Candidatein the Nearby TW Hydrae Association. The Astrophysical Journal Letters **512**, L63 (1999).

[3] Sterzik, M. F., Alcalá, J. M., Covino, E. & Petr, M. G. New T Tauri stars in the vicinity of TW Hydrae. Astronomy and Astrophysics **346**, L41-L44 (1999).

[4] Zuckerman, B., Song, I. & Webb, R. Tucana Association. The Astrophysical Journal **559**, 388 (2001).

[5] Song, I., Zuckerman, B. & Bessell, M. New Members of the TW Hydrae Association, β Pictoris Moving Group, and Tucana/Horologium Association. The Astrophysical Journal **599**, 342 (2003).

[6] Van Leeuwen, F. Validation of the new Hipparcos reduction. Astronomy & Astrophysics **474**, 653-664 (2007).

[7] Alencar, S. H. & Batalha, C. Variability of southern T Tauri stars. II. The spectral variability of the classical T Tauri star TW Hydrae. The Astrophysical Journal **571**, 378 (2002).

[8] Rosenfeld, K. A., Andrews, S. M., Wilner, D. J. & Stempels, H. A disk-based dynamical mass estimate for the young binary V4046 Sgr. The Astrophysical Journal **759**, 119 (2012).

[9] Thi, W.-F., Van Zadelhoff, G.-J. & van Dishoeck, E. F. Organic molecules in protoplanetary disks around T Tauri and Herbig Ae stars. Astronomy & Astrophysics **425**, 955-972 (2004).

[10] Qi, C. et al. Imaging the disk around TW Hydrae with the submillimeter array. The Astrophysical Journal Letters **616**, L11 (2004).

[11] Qi, C. et al. CO J= 6-5 observations of TW Hydrae with the Submillimeter Array. The Astrophysical Journal Letters **636**, L157 (2006).

[12] Qi, C. et al. Resolving the CO snow line in the disk around HD 163296. The Astrophysical Journal **740**, 84 (2011).

[13] Rodriguez, D. R., Kastner, J. H., Wilner, D. & Qi, C. Imaging the Molecular Disk Orbiting the Twin Young Suns of V4046 Sgr. The Astrophysical Journal **720**, 1684 (2010).

[14] Andrews, S. M. et al. Ringed substructure and a gap at 1 au in the nearest protoplanetary disk. The Astrophysical Journal Letters **820**, L40 (2016).

[15] Rosenfeld, K. A., Andrews, S. M., Wilner, D. J., Kastner, J. & McClure, M. The structure of the evolved circumbinary disk around V4046 Sgr. The Astrophysical Journal **775**, 136 (2013).

[16] Menu, J. et al. On the structure of the transition disk around TW Hydrae. Astronomy & Astrophysics **564**, A93 (2014).

[17] Aikawa, Y., Furuya, K., Nomura, H. & Qi, C. Analytical Formulae of Molecular Ion Abundances and the N2H+ Ring in Protoplanetary Disks. The Astrophysical Journal 807, 120 (2015).

[18] Rapson, V. A., Kastner, J. H., Millar-Blanchaer, M. A. & Dong, R. Peering into the Giant-planet-forming Region of the TW Hydrae Disk with the Gemini Planet Imager. The Astrophysical Journal Letters **815**, L26 (2015).

[19] Debes, J. H., Jang-Condell, H. & Schneider, G. The inner structure of the TW Hya Disk as revealed in scattered light. The Astrophysical Journal Letters **819**, L1 (2016).

[20] Wilner, D. J., D'Alessio, P., Calvet, N., Claussen, M. & Hartmann, L. Toward planetesimals in the disk around TW Hydrae: 3.5 centimeter dust emission. The Astrophysical Journal Letters **626**, L109 (2005).

[21] Testi, L., Natta, A., Shepherd, D. & Wilner, D. Large grains in the disk of CQ Tau. Astronomy & Astrophysics **403**, 323-328 (2003).

[22] Calvet, N. et al. Evidence for a developing gap in a 10 Myr old protoplanetary disk. The Astrophysical Journal **568**, 1008 (2002).

[23] Hughes, A. et al. An inner hole in the disk around TW Hydrae resolved in 7 mm dust emission. The Astrophysical Journal **664**, 536 (2007).

[24] Debes, J. H., Jang-Condell, H., Weinberger, A. J., Roberge, A. & Schneider, G. The 0.5-2.22 micrometer Scattered Light Spectrum of the Disk around TW Hya: Detection of a Partially Filled Disk Gap at 80 AU. (2013).

[25] Akiyama, E. et al. Discovery of a disk gap candidate at 20 AU in TW Hydrae. The Astrophysical Journal Letters **802**, L17 (2015).

[26] Wilner, D., Ho, P., Kastner, J. & Rodríguez, L. VLA imaging of the disk surrounding the nearby young star TW Hydrae. The Astrophysical Journal Letters **534**, L101 (2000).

[27] Hughes, A. M., Wilner, D. J., Andrews, S. M., Qi, C. & Hogerheijde, M. R. Empirical constraints on turbulence in protoplanetary accretion disks. The Astrophysical Journal **727**, 85 (2011).

[28] Ruane, G. et al. Deep imaging search for planets forming in the TW Hya protoplanetary disk with the Keck/NIRC2 vortex coronagraph. The Astronomical Journal **154**, 73 (2017).

[29] Andrews, S. M. et al. The TW Hya disk AT 870 μm: Comparison of co and dust radial structures. The Astrophysical Journal **744**, 162 (2011).

[30] Rodriguez, D. R. et al. An ALMA survey for disks orbiting low-mass stars in the TW Hya Association. Astronomy & Astrophysics **582**, L5 (2015).

[31] Lada, C. J. in Symposium-International Astronomical Union. 1-18 (Cambridge University Press).

[32] Robitaille, T. P. HYPERION: an open-source parallelized three-dimensional dust continuum radiative transfer code. Astronomy & Astrophysics **536**, A79 (2011).

[33] Draine, B. T. Interstellar dust grains. Annual Review of Astronomy and Astrophysics **41**, 241-289

(2003).

[34] Cleeves, L. I., Bergin, E. A., Qi, C., Adams, F. C. & Öberg, K. I. Constraining the X-ray and cosmic-ray ionization chemistry of the TW Hya protoplanetary disk: evidence for a sub-interstellar cosmic-ray rate. The Astrophysical Journal **799**, 204 (2015).

[35] Huang, J. et al. CO and dust properties in the TW Hya disk from high-resolution ALMA observations. The Astrophysical Journal **852**, 122 (2018).

[36] Nomura, H. et al. ALMA observations of a gap and a ring in the protoplanetary disk around TW Hya. The Astrophysical Journal Letters **819**, L7 (2016).

[37] Bergin, E. A. et al. An old disk still capable of forming a planetary system. Nature **493**, 644 (2013).

[38] Favre, C., Cleeves, L. I., Bergin, E. A., Qi, C. & Blake, G. A. A Significantly Low CO Abundance Toward the TW Hya Protoplanetary Disk: A Path to Active Carbon Chemistry? The Astrophysical Journal Letters **776**, L38 (2013).

[39] Williams, J. P. & Best, W. M. A parametric modeling approach to measuring the gas masses of circumstellar disks. The Astrophysical Journal **788**, 59 (2014).